Geophysical Research Letters

Supporting Information for

Updated Models of Current Sheet and Magnetic Field in the Jovian Magnetosphere for Pre-Galileo, Galileo and Juno Eras

Naoya Momoki[1] and Hiroaki Toh[2]

[1] Division of Earth and Planetary Sciences, Graduate School of Science, Kyoto University

[2] Data Analysis Center for Geomagnetism and Space Magnetism, Graduate School of Science, Kyoto University

Contents of this file

Introduction

This supplement provides two additional descriptions about the CS shape and magnetospheric filed model parameters and eight figures in order to show the detailed characteristics of the models updated in this study. The additional texts describe the parameterization of the two models and meaning of the model parameters. Text 1 is for the CS shape model, and Text 2 is for the magnetospheric field model. The current sheet has two characteristics as mentioned in the main text, namely, bendback and hinge. Figure S1 represents comparison of the bendback effect with δ in Eq. (1). Figure S2 represents comparison of the hinge effect in the midnight meridional plane where the effect becomes most prominent. Figure S3 shows the comparison of the magnetospheric field model parameters among the three models (pre-Galileo, Galileo, and Juno) with parameter error estimates based on the observation errors. Figures S4 through S6 indicate the stability of the updated magnetospheric field model by showing the RMS curves in the vicinity of the optimized parameters listed in Table 1 of the main text. These figures are for pre-Galileo, Galileo and Juno, respectively. Figures S7 and S8 represent the calculated azimuthal electric current density using the field models updated in this study for Galileo and Juno, respectively.

Text S1.

In this text, the CS shape model parameters (x_0, ρ_0, v_0) are described in detail.

The x_0 controls the hinge effect mentioned in the main text through the term in Eq. (1):

$$\rho \frac{x_0}{x} \tanh\left(\frac{x}{x_0}\right). \tag{S1}$$

First, considering the dawn-dusk meridian, $x = 0$ and $\rho = |y|$, which is dusk-directional distance on the equatorial plane. In the case of $|x| \ll |x_0|$, by using an approximation,

$$\tanh\left(\frac{x}{x_0}\right) \simeq \frac{x}{x_0}, \tag{S2}$$

the term (S1) becomes a simpler form:

$$\rho \frac{x_0}{x} \tanh\left(\frac{x}{x_0}\right) \simeq |y| \quad . \tag{S3}$$

The CS shape model (1), therefore, can be simplified:

$$Z_{CS} \simeq |y| \tan(\theta_d) \cos(\lambda - \delta)\,. \tag{S4}$$

This means that the Z-coordinate of the CS is not constrained by ρ in this meridian. Next, on the midnight meridian where $\rho = -x$, the CS shape model (1) becomes

$$Z_{CS} = -\tan(\theta_d)\, x_0 \tanh\left(\frac{x}{x_0}\right) \cos(\lambda - \delta)\,. \tag{S5}$$

While in the case of $|x| \ll |x_0|$ (i.e. near Jupiter), (S5) can be simplified to the same form as (S4):

$$Z_{CS} \simeq -x \tan(\theta_d) \cos(\lambda - \delta) \quad , \tag{S6}$$

in the case of $|x| \gg |x_0|$ (i.e., distant from Jupiter), the hyperbolic tangent term becomes unity and the Z-coordinate of the CS is independent of ρ:

$$Z_{CS} = -\tan(\theta_d)\, x_0 \cos(\lambda - \delta) \quad . \tag{S7}$$

This means the Z-coordinate is saturated with large x, and x_0 is the scale distance where the hinge effect becomes dominant and rules the maximum height of the CS ($\tan(\theta_d)\,|x_0|$).

On the other hand, ρ_0 and v_0 control the bendback effect mentioned in the main text through the term:

$$\frac{\Omega_J \rho_0}{v_0} \ln\cosh\left(\frac{\rho}{\rho_0}\right) \quad . \tag{S8}$$

While δ in Eq. (1) means the longitude at which the CS has the maximum tilt without

the hinge effect, it isn't equal to the longitude at which the Jupiter's dipole points, λ_d. δ varies as a function of ρ corresponding to the finite propagation velocity of the CS oscillation originated from the rotation of Jupiter's dipole. The difference between the longitudes, therefore, can be formulated in an integral form:

$$\delta - \lambda_d = \Omega_J \int_0^{\rho} \frac{d\rho}{v(\rho)} \tag{S9}$$

where v is the propagation velocity as the function of ρ. In this model, the velocity is modeled by using the hyperbolic tangent:

$$v(\rho) = \frac{v_0}{\tanh\left(\frac{\rho}{\rho_0}\right)}, \tag{S10}$$

and by integrating it, δ in Eq. (1) can be obtained. In the case of $\rho \ll \rho_0$, $v(\rho)$ diverges to infinity with the approximation (S2), and this corresponds to no bendback effect near Jupiter because of the infinite propagation velocity. In a contrasting situation, $\rho \gg \rho_0$, the velocity reaches a constant value, v_0. It follows that ρ_0 controls the distance where the bendback effect becomes dominant, and v_0 rules the strength of the effect.

Text S2.

In this text, we will explain what the magnetospheric field model parameters means.

The magnetospheric field model is formulated by the Euler potentials f and g that are the functions of the spatial coordinates (ρ_m, ϕ, Z_m):

$$\begin{aligned} \boldsymbol{B} &= \boldsymbol{\nabla} f(\rho_m, \phi, Z_m) \times \boldsymbol{\nabla} g(\rho_m, \phi, Z_m), \\ B_{\rho_m} &= \frac{\partial f}{\rho_m \partial \phi}\frac{\partial g}{\partial Z_m} - \frac{\partial f}{\partial Z_m}\frac{\partial g}{\rho_m \partial \phi}, \\ B_{\phi} &= \frac{\partial f}{\partial Z_m}\frac{\partial g}{\partial \rho_m} - \frac{\partial f}{\partial \rho_m}\frac{\partial g}{\partial Z_m}, \\ B_{Z_m} &= \frac{\partial f}{\partial \rho_m}\frac{\partial g}{\rho_m \partial \phi} - \frac{\partial f}{\rho_m \partial \phi}\frac{\partial g}{\partial \rho_m}. \end{aligned} \tag{S11}$$

The formulation using the Euler potentials was obtained as follows. The observed B_{ρ_m} and B_{Z_m} were well explained by their zeroth-order approximations (Khurana, 1997), $B_{\rho_m 0}$ and $B_{Z_m 0}$:

$$
\begin{aligned}
B_{\rho_m 0} &= C_1 \left\{ \tanh\left(\frac{\rho_{01}}{\rho_m}\right) \right\}^{a_1} \tanh\left(\frac{Z_m}{D_1}\right), \\
B_{Z_m 0} &= C_2 \left\{ \tanh\left(\frac{\rho_{02}}{\rho_m}\right) \right\}^{a_2} + C_3 \left\{ \tanh\left(\frac{\rho_{03}}{\rho_m}\right) \right\}^{a_3} + C_4.
\end{aligned}
\tag{S12}
$$

Assuming a Euler potential g_0, the zeroth-order approximation of the g, is equal to ϕ, $B_{\rho_m 0}$, $B_{Z_m 0}$, and $B_{\phi 0}$ (the zeroth-order approximation of the B_ϕ) can be expressed by f_0, the zeroth-order approximation of the f:

$$
\begin{aligned}
B_{\rho_m 0} &= -\frac{1}{\rho_m}\frac{\partial f_0}{\partial Z_m} \quad , \\
B_{\phi 0} &= 0 \quad , \\
B_{Z_m 0} &= \frac{1}{\rho_m}\frac{\partial f_0}{\partial \rho_m} \quad .
\end{aligned}
\tag{S13}
$$

Using (S12) and (S13), f_0 can be obtained:

$$
\begin{aligned}
f_0 &= -\int \rho_m B_{\rho_m 0} dZ_m + \int \rho_m B_{Z_m 0} d\rho_m \\
&= -C_1 \rho_m \left\{ \tanh\left(\frac{\rho_{01}}{\rho_m}\right) \right\}^{a_1} \ln\cosh\left(\frac{Z_m}{D_1}\right) \\
&\quad + \int \rho_m \left\{ C_2 \left\{ \tanh\left(\frac{\rho_{02}}{\rho_m}\right) \right\}^{a_2} + C_3 \left\{ \tanh\left(\frac{\rho_{03}}{\rho_m}\right) \right\}^{a_3} + C_4 \right\} d\rho_m \quad .
\end{aligned}
\tag{S14}
$$

where the term $C_1 D_1$ emerged by the integration is redefined as the C_1. In Khurana (1997), Z_m was modified to $Z_m - Z_{m,CS}$ corresponding to the complex shape of the current sheet, and ρ_{01}/ρ_m was replaced by r_{01}/r.

The parameter C_1 (more precisely, C_1/D_1) and C_2 through C_4 represent the B_ρ and the components of the B_{Z_m} at $\rho_m = 0$. Furthermore, considering the approximation of the hyperbolic tangent (S2) where $\rho_m \gg \rho_0$, a_1 through a_3 represent the powers with which each component decreases, and r_{01}, ρ_{02}, and ρ_{03} represent the scale distances where the power law become significant. D_1 is regarded as the Z_m-directional distance where the B_{ρ_m} is saturated with increasing $Z_m - Z_{m,CS}$.

g can be obtained by adding the bendback effect of the magnetic field to the g_0 and it is formulated as the second term of Eq. (2). Considering the typical values of the p and q are both positive, the term increases and ϕ decreases with increasing ρ_m on a magnetic field line in order to conserve the Euler potential g. The parameters p, q, and D_2 are regarded as the bendback rate against ρ_m at the center of the CS, the increment of the bendback rate with increasing $Z_m - Z_{m,CS}$, and the Z_m-directional distance where the effect of q is saturated.

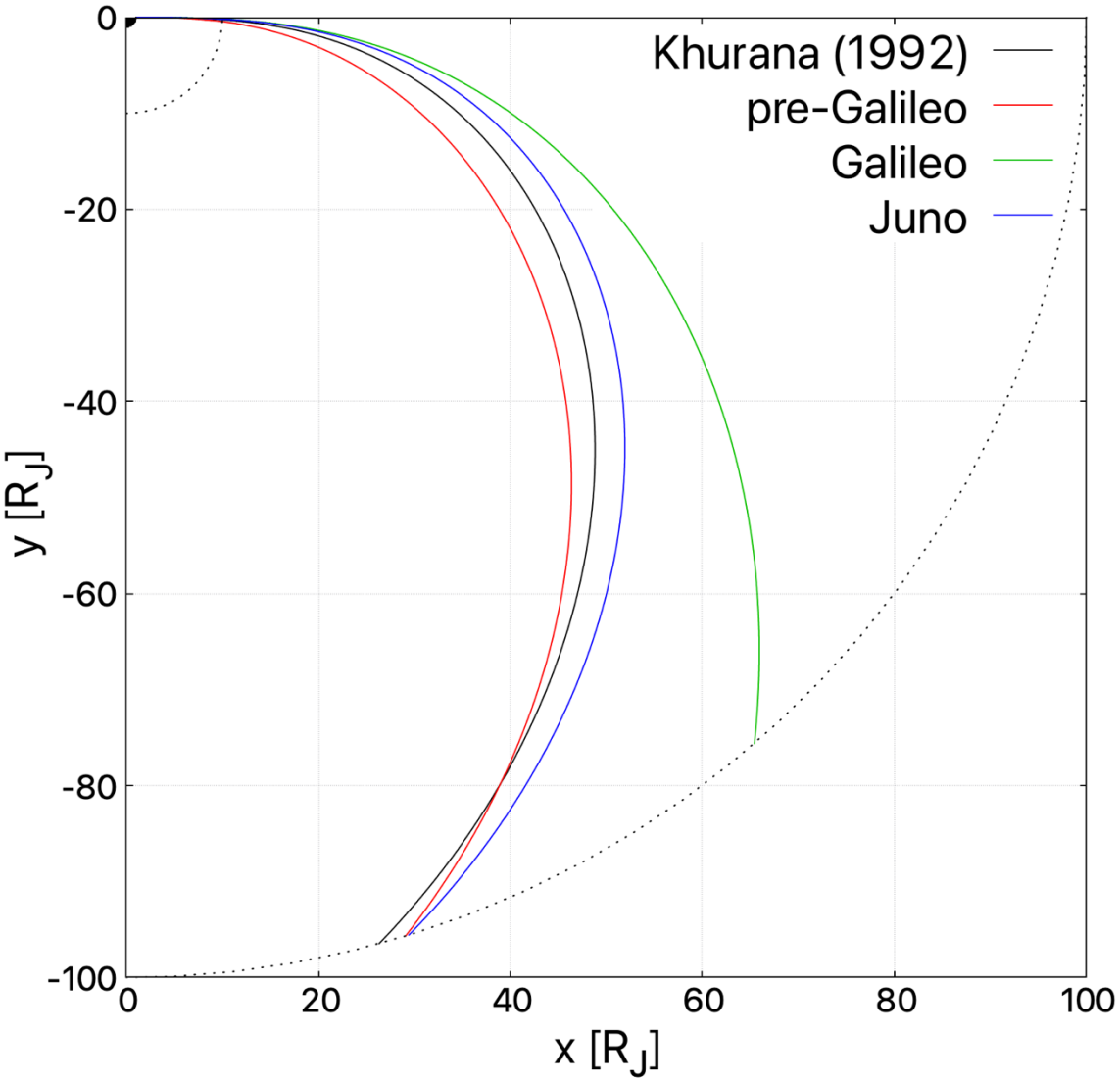

Figure S1. Comparison of the bendback effect of the CS shape models on the Jovigraphical equatorial plane with the System III longitude $\boldsymbol{\lambda = \lambda_d}$ as $\boldsymbol{x}$-axis. The $\boldsymbol{x}$ and $\boldsymbol{y}$ distances are measured in units of $\boldsymbol{R_J}$. Each curve represents the modeled $\boldsymbol{\delta}$ of Khurana (1992) (black), pre-Galileo (red), Galileo (green) and Juno (blue). The black area at the origin represents Jupiter and the two dotted circles represent the distance range of the used data (10 $\boldsymbol{R_J}$ and 100 $\boldsymbol{R_J}$ from the origin, respectively).

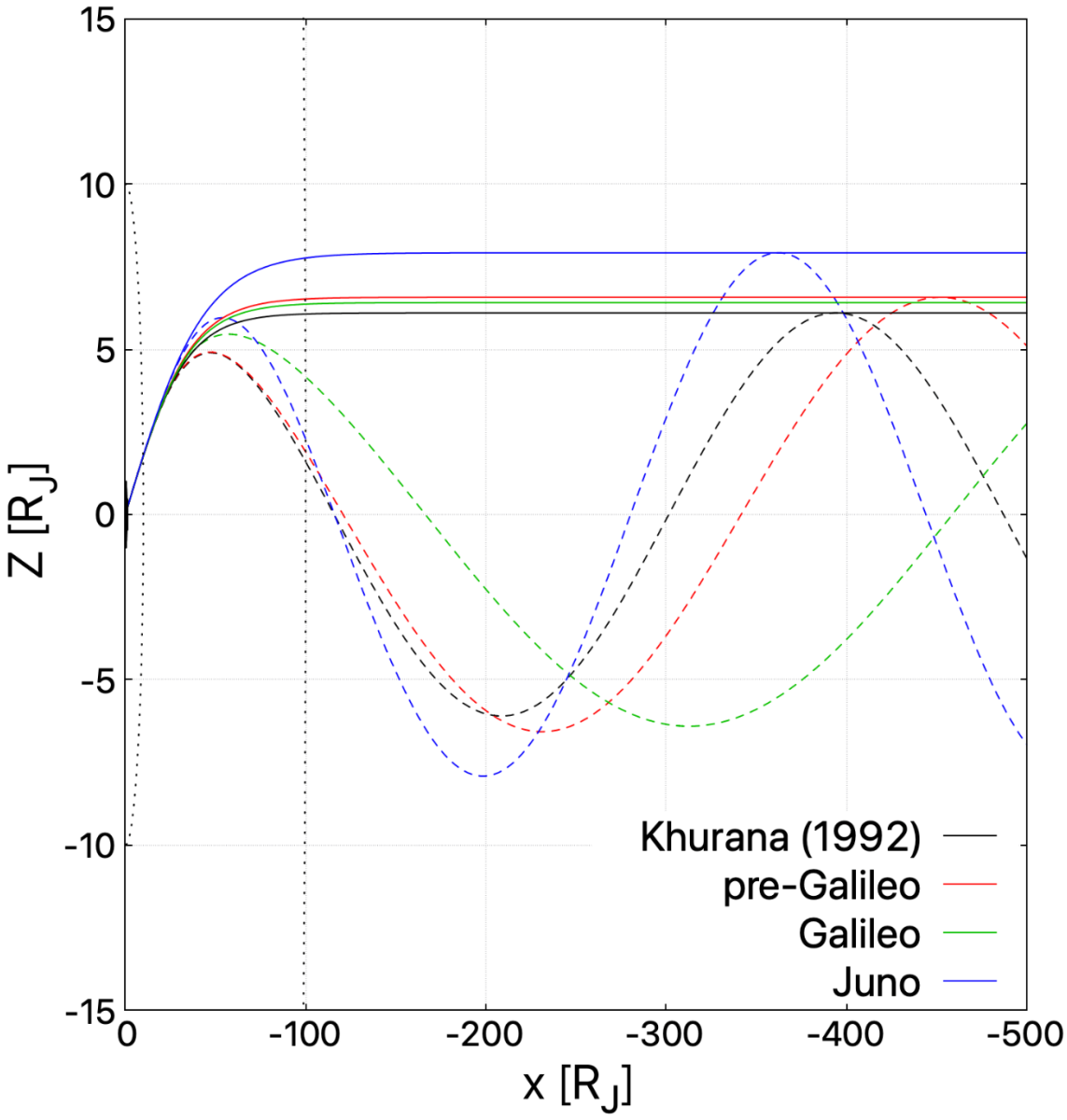

Figure S2. Comparison of the hinge effect of the CS shape models in the Jovigraphical midnight meridional plane whose distances are measured in $\boldsymbol{R_J}$ with sunward direction as $\boldsymbol{x}$-axis. Dashed curves represent cross-sections of the CSs in the midnight meridian whose System III longitude $\boldsymbol{\lambda}$ is $\boldsymbol{\lambda_d}$, while solid curves denote those in the pseudo prime meridian ($\boldsymbol{\lambda = \delta}$) at midnight. The colors corresponding to the models are the same as Figure S1. Black dotted curves represent the distance range of the used data.

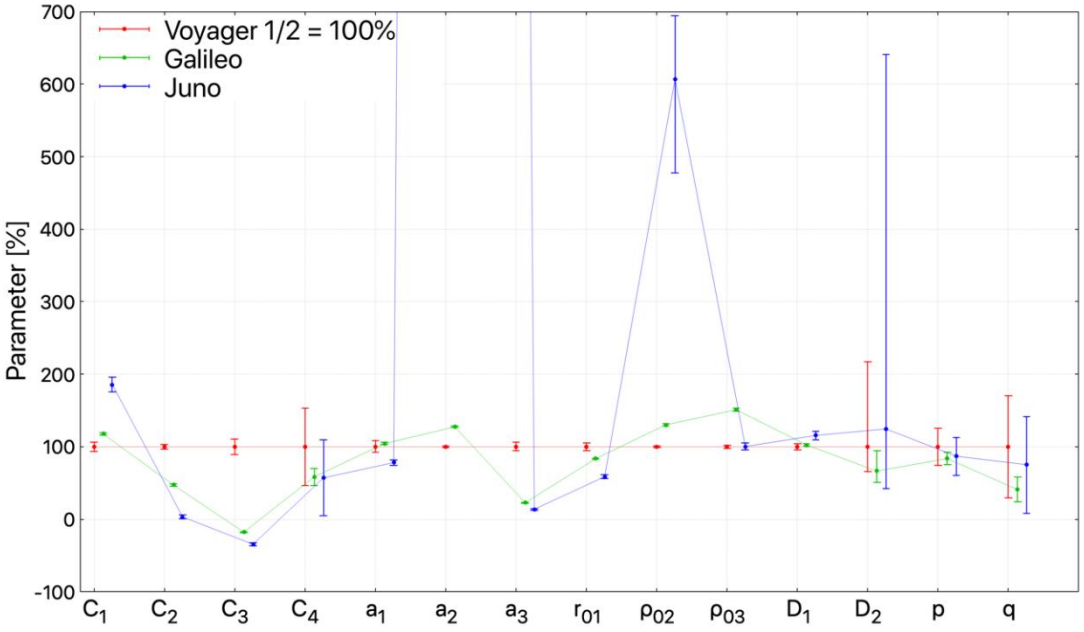

Figure S3. The updated parameters normalized by each pre-Galileo parameter and their estimated errors. Red, blue and green parameters represent those in pre-Galileo (Voyager 1/2), Galileo and Juno models, respectively. The errors are estimated based on the errors of the observed magnetic field.

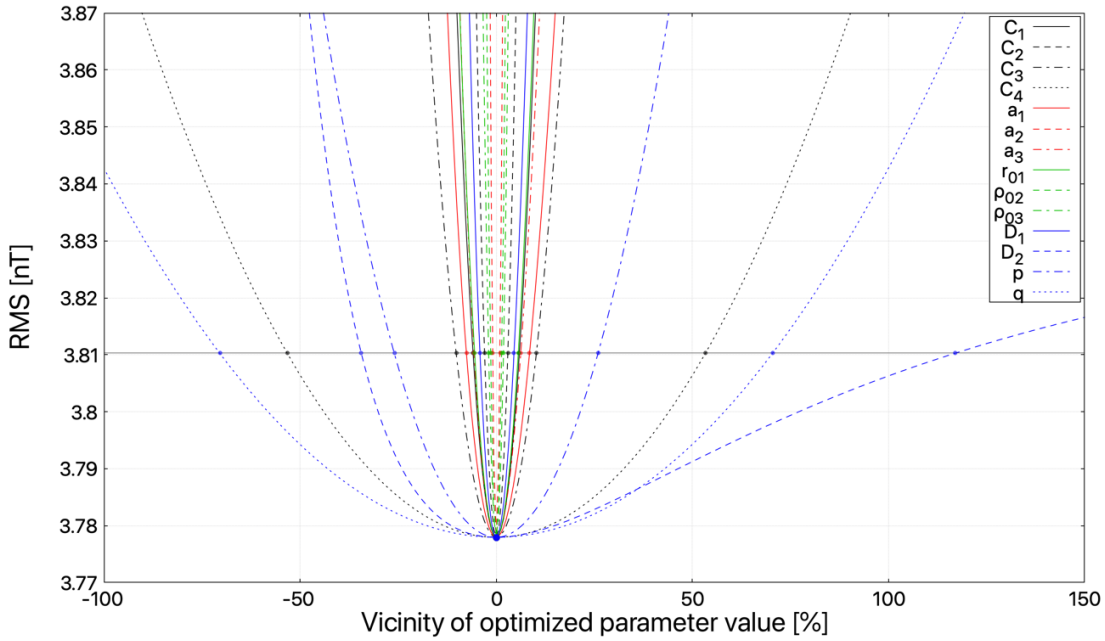

Figure S4. The RMS distributions in the vicinity of each updated magnetospheric model parameter in the pre-Galileo era listed in Table 1. The horizontal line represents the possible RMS value when the observation errors are considered, and the cross points with each curve correspond to each error bar in the Figure S3.

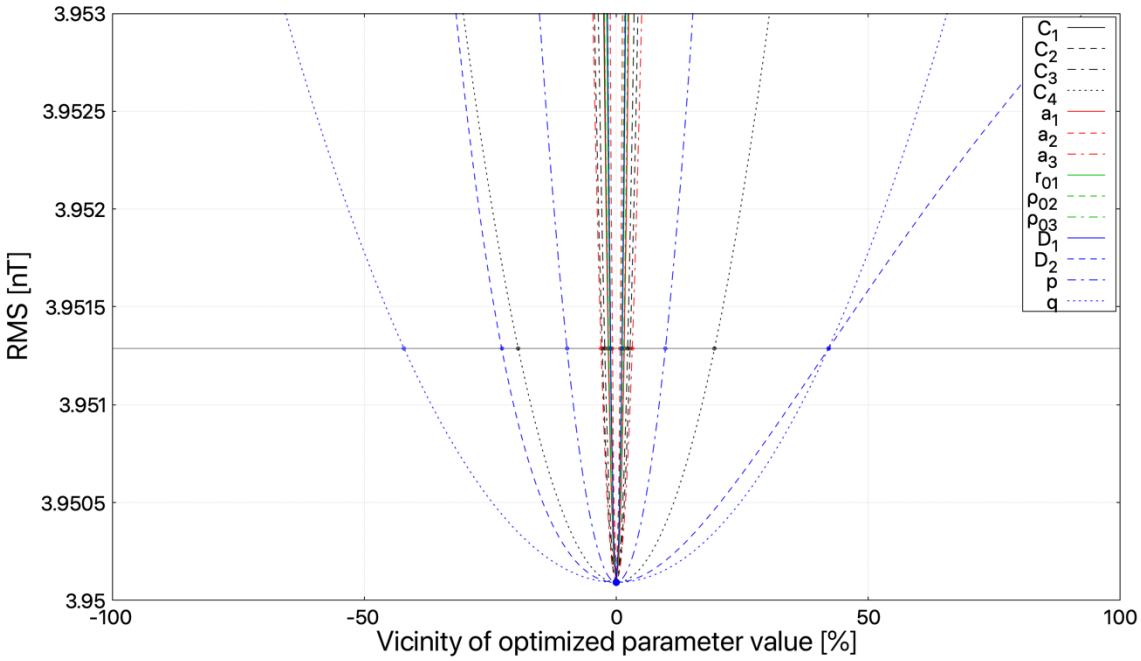

Figure S5. The RMS distributions in the vicinity of each updated magnetospheric model parameter in the Galileo era listed in Table 1. The figure format is same as Figure S4.

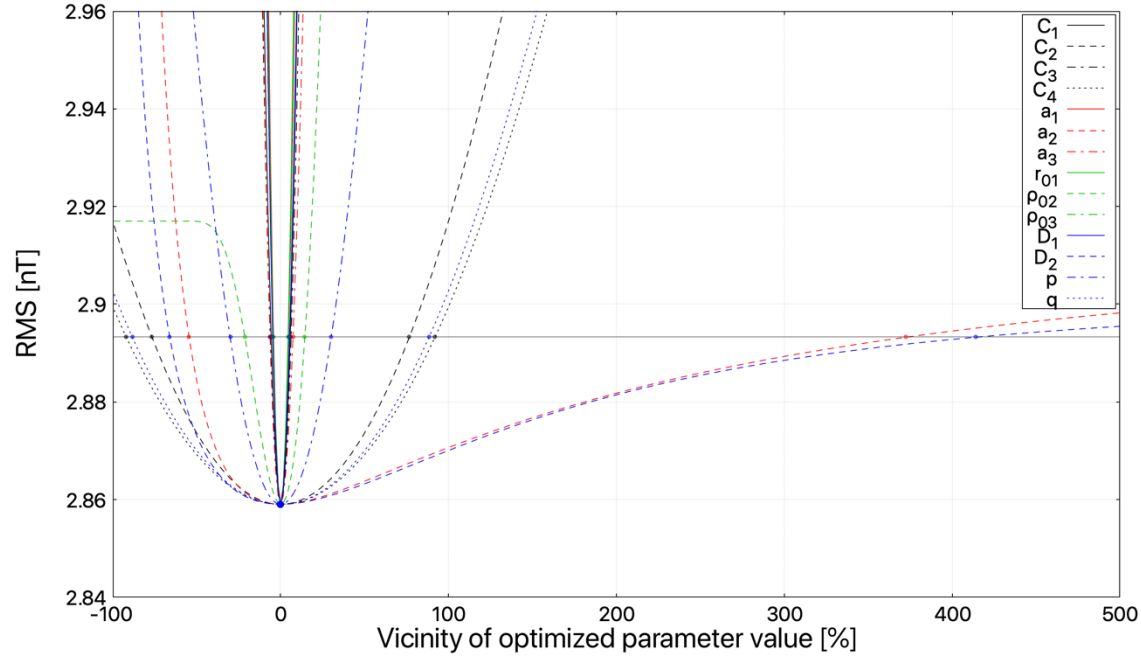

Figure S6. The RMS distributions in the vicinity of each updated magnetospheric model parameter in the Juno era listed in Table 1. The figure format is same as Figure S4.

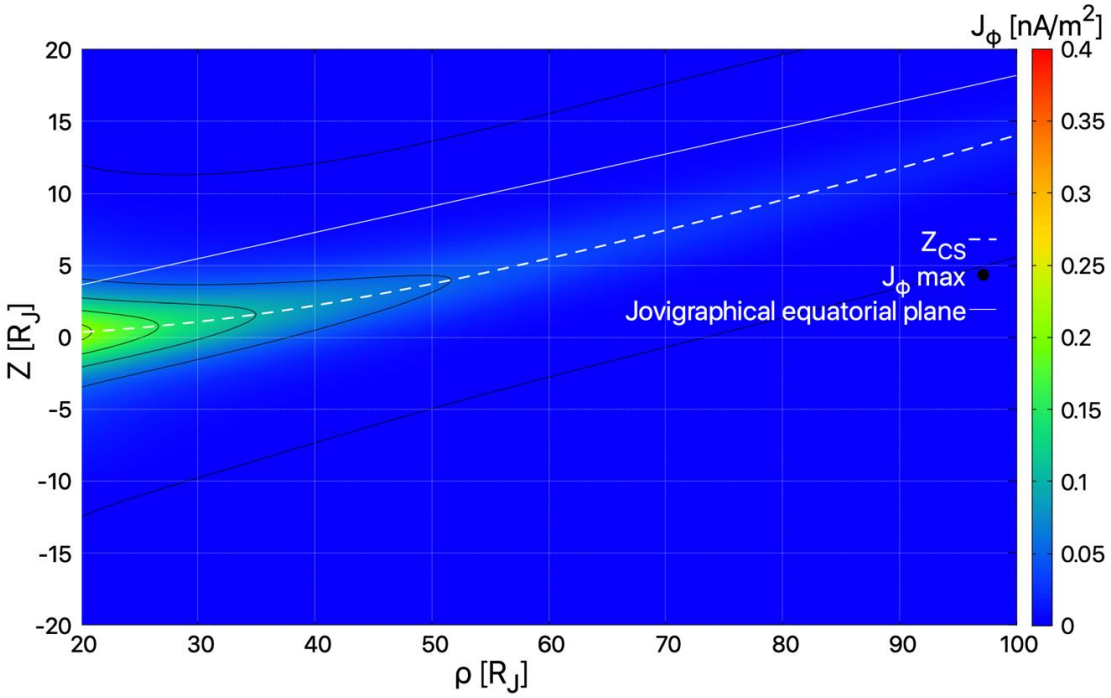

Figure S7. The azimuthal electric current density calculated by the updated magnetospheric field model in the Galileo era on the midnight meridian using the magnetic dipole coordinate system. The solid and dashed white lines represent the cross-sections of the Jovigraphical equator and modeled CS on this meridian.

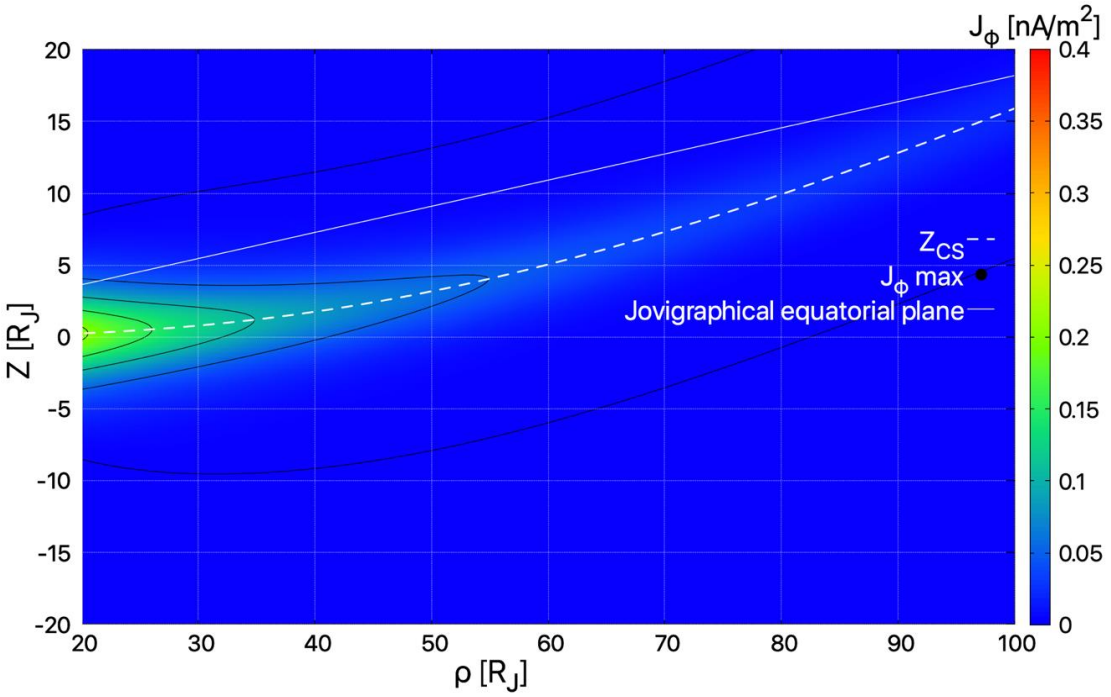

Figure S8. The azimuthal electric current density calculated by the updated magnetospheric field model in the Juno era. The figure format is same as Figure S7.